SPIN
Vol. 2, No. 4 (2012) 1230004 (18 pages)

DOI: 10.1142/S2010324712300046

World Scientific
www.worldscientific.com

PROGRESS ON ANISOTROPIC MAGNETORESISTANCE EFFECT IN PEROVSKITE MANGANITES

HUALI YANG, YIWEI LIU and RUN-WEI LI*
Key Laboratory of Magnetic Materials and Devices
Ningbo Institute of Material Technology and Engineering (NIMTE)
Chinese Academy of Sciences (CAS)
Ningbo 315201, People's Republic of China

Zhejiang Province Key Laboratory of Magnetic
Materials and Application Technology
Ningbo Institute of Material Technology and Engineering (NIMTE)
Chinese Academy of Sciences (CAS)
Ningbo, 315201, People's Republic of China
**runweili@nimte.ac.cn*

Received 23 January 2013
Accepted 31 January 2013
Published 4 March 2013

Anisotropic magnetoresistance (AMR) effect has been discovered over one century, but keeps attracting people's special attention due to its wide applications in magnetic devices as well as its intimate relationship with the most fascinating physics such as spin−orbit interaction and spin−charge coupling. In this review article, we introduce the general characters and tuning methods of AMR effect in perovskite manganites, the typical strongly correlated electron system, and discuss the possible mechanisms behind. Outlooks of the AMR effects in manganites and related devices are also addressed.

Keywords: Anisotropic magnetoresistance; perovskite manganites; correlated electron system; spin−orbit coupling.

1. Introduction

Anisotropic magnetoresistance (AMR) effect is the phenomenon that the electrical resistivity of a substance depends on the direction of external magnetic field. If the magnetization ($\mathbf{M}$) makes an angle θ with the current, then the AMR curve $\rho(\theta)$ gives a good recording of the magnetization direction-dependent resistivity. The AMR value is usually defined as:

$$\mathrm{AMR} = \frac{\rho_{\parallel} - \rho_{\perp}}{\frac{1}{3}\rho_{\parallel} + \frac{2}{3}\rho_{\perp}}, \tag{1}$$

where $\rho_{\parallel}$ and $\rho_{\perp}$ correspond to the resistivities when magnetization is oriented parallel and perpendicular to the direction of current, respectively.

*Corresponding author.

Following the pioneering work by Lord Kelvin in 1857,[1] intensive studies of the AMR effect has been conducted in $3d$ ferromagnets[2–5] (mainly in polycrystalline form). According to the experimental results, the AMR value is generally, but not always, positive. Negative AMR values were found in materials such as Fe_4N[6] and some Ir doped transitional metals.[3] The AMR effect in $3d$ ferromagnets usually increases into saturation with the increase of magnetic field strength,[2] and shows a decreasing trend with increasing the temperature.[7]

In polycrystalline samples, the AMR effect can be understood phenomenologically from symmetry considerations,[8,9] based on which the relationship between the electrical field ($\mathbf{E}$) and the current density ($\mathbf{J}$) can be expressed as:

$$\mathbf{E} = \rho_{\perp}(M)\mathbf{J} + \rho_H(M)\boldsymbol{\alpha} \times \mathbf{J} + [\rho_{\parallel}(M) - \rho_{\perp}(M)][\boldsymbol{\alpha} \cdot \mathbf{J}]\boldsymbol{\alpha}, \quad (2)$$

where $\boldsymbol{\alpha}$ denotes the unit vector along the magnetization direction, and $\rho_H(M)$ is the hall resistivity. From Eq. (2), we can derivate:

$$\rho(\theta) = \rho_{\perp} + (\rho_{\parallel} - \rho_{\perp})\cos^2\theta, \quad (3)$$

which means $\rho(\theta)$ is proportional to $\cos^2\theta$, this relationship fits quite well with most of the experimental results.

As for the microscopic origin of the AMR effect in $3d$ ferromagnets, Mott reported[10] that the resistivity in $3d$ ferromagnets is mainly caused by the $s-d$ scattering, and the scattering rate is spin dependent. Based on this model, Smit proposed[11] that the spin–orbit (SO) coupling of d electrons breaks the cubic symmetry of a crystal lattice, and the $s-d$ scattering rate becomes sensitive to the spin orientation, which causes the AMR effect. These theoretical works has greatly improved the understanding of AMR effect in $3d$ ferromagnets.[2]

As the spin orientation in $3d$ ferromagnets can be easily affected by a small external magnetic field, sensors based on the AMR effect can provide high resolution of the magnetic field as well as its direction. Typical applications of the AMR sensors include magnetic read heads, automotive wheel speed and crankshaft sensing, vehicle detection, compass navigation, and current sensing, etc. AMR sensors possess many advantages such as low cost, noise immunity, and good reliability, however, their magnetic sensitivity is lower than that based on giant magnetoresistance (GMR) effect[12,13] and tunneling magnetoresistance (TMR) effect.[14] In order to obtain a large AMR value, studies of the AMR effect in low dimensional structures[15–18] and new materials[19–29] have been widely conducted.

The AMR effect in low dimensional structures can exhibit very unusual behaviors.[15,30] For example, the AMR in a quantum point contact shows stepwise periodic variations in the conductance with varying the field direction,[30] which is called ballistic anisotropic magnetoresistance (BAMR) effect. Single electronic transistors (SET) based on ferromagnetic materials exhibit coulomb blockade anisotropic magnetoresistance (CBAMR) effect,[17] where the resistivity of SET strongly depends on the magnetic orientation.

The AMR effect has been studied in some new material systems, including graphene,[19] topological insulators,[21,22] ferromagnetic semiconductors,[31–33] and electron correlation systems such as superconductors,[25,26,34,35] heavy fermions,[24] manganites,[27,29,36] etc.[37–40] For example, in graphene, the magnetoresistance (MR) value is high for magnetic field perpendicular to the graphene plane, while there is little resistance change for magnetic field applied in the film plane.[19,41] Similar behavior was found in topological insulator Bi_2Se_3 nanoribbons.[23] When the magnetic field is applied perpendicular to the surface of the Bi_2Se_3 nanoribbons, MR is found to be large, while for field applied parallel to the surface, the MR effect is negligibly small. In ferromagnetic semiconductors, giant anisotropic MR effect has been found in ultrathin (Ga, Mn)As films with metal–insulator transition,[33] reaching a value as high as 50% in the insulating state. In electron correlated systems, the AMR effect shows very complex behaviors. For example, the in-plane (i.e., the CuO_2 plane) AMR of bilayered $Pr_{1.3-x}La_{0.7}Ce_xCuO_4$ single crystals[38] exhibits intriguing fourfold-symmetric angular dependence even when collinear spin arrangement in adjacent CuO_2 planes is achieved. This obviously cannot originate from the spin-valve effects and indicates a strong spin–charge coupling in this electron-doped cuprates.[38] The AMR effect in perovskite manganites has attracted a lot of attention[20,27,29,42–45] because these materials may provide a path to achieve large AMR values near room temperature. For example, the AMR value in $La_{0.69}Ca_{0.31}MnO_3$ single crystals can reach as high as 90% at 220 K under a magnetic field of about 0.2 Tesla.[29] Investigations on the AMR effect in perovskite manganites have been intensively conducted

in order to understand the physics behind, and provide guidance for the design of new materials that may exhibit large AMR value at room temperature. In this review article, we will focus on the AMR effect in perovskite manganites.

2. AMR Effect in Perovskite Manganites

2.1. *Introduction of the perovskite manganites*

Most of the manganites possess the perovskite structure. The size mismatch between the A-site ion (RE^{3+} and AE^{2+}) and B-site manganese usually cause compressive strain of the Mn−O bonds and tensile strain of the A−O bonds, which are alleviated through a cooperative rotation of the MnO_6 octahedra. For example, in the orthorhombic structure, the MnO_6 octahedra will tilt from the c-axis and simultaneously rotate in the $a-b$ plane, as schematically shown in Fig. 1.

In perovskite manganites, the transition metal Mn is surrounded by six oxygen ions, and the crystal field around each Mn splits its $3d$ levels into a lower energy t_{2g} triplets ($d$xy, $d$yz, and $d$zx orbitals) and a higher energy e_g doublets (dx^2-y^2 and $d3z^2$-r^2 orbitals). Because of Hund's rule, all the spins of t_{2g} and e_g electrons are aligned parallel, forming an $S = 3/2$ spin state for the Mn^{4+} ions and $S = 2$ state for the Mn^{3+} ions. For Mn^{3+} ions (such as in $LaMnO_3$), there are four electrons in its d orbitals, three of which will occupy the t_{2g} orbitals and the fourth electron will stay in e_g orbitals. Because each orbit has a different anisotropy of the wave function, depending on which orbit the fourth electron stay, there will be a corresponding lattice distortion in order to minimize the total energy, which is called the Jahn−Teller (JT) effect. The d electron splitting along with the JT effect is schematically shown in Fig. 2.

Manganites belong to the strongly correlated electron materials, where the electron−electron Coulomb repulsion force plays a significant role in determining the band structure. The electron hopping amplitude t competes with the electron−electron Coulomb repulsion energy U and the outcome of this competition is the metal−insulator transition (MIT). As can be seen from Fig. 3, there

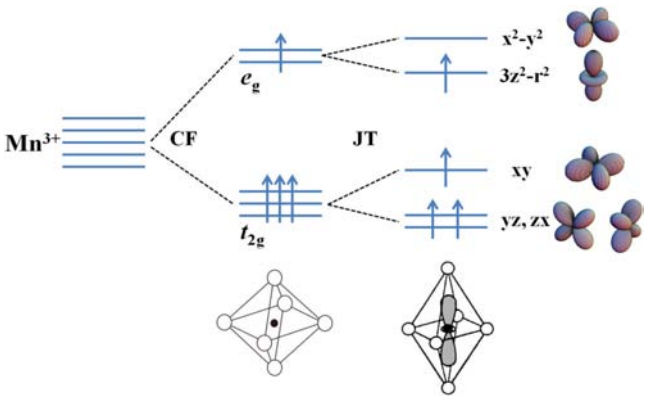

Fig. 2. Schematic electronic structure of M^{3+} ion in MnO_6 octahedron with JT distortion.

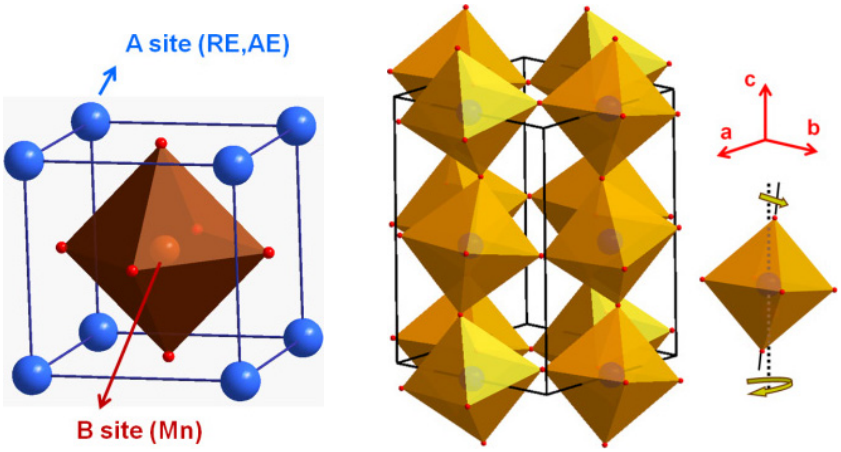

(a) (b)

Fig. 1. (a) The ideal cubic perovskite structure of manganites. (b) Orthorhombically distorted structure of the perovskite manganites.

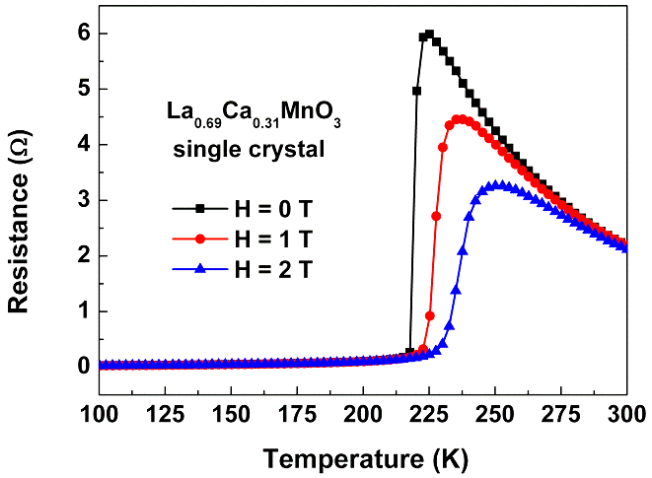

Fig. 3. Metal−insulator transition behavior for the $La_{0.69}Ca_{0.31}MnO_3$ single crystal with $H = 0$, 1, and 2 T.

is a huge resistance change through the metal−insulator transition temperature (T_{MI}). The fundamental parameters for controlling the physical properties in perovskite manganites include the one-electron bandwidth (depending on the Mn−O bond length and Mn−O−Mn bond angle) and the band filling (depending on the density of charge carriers), which can be efficiently controlled through the chemical doping.

The spin, orbital and charge ordered phases[46–49] revealed in the phase diagrams (some of them are shown in Fig. 4) manifest a complexity of the competing forces inside this system. Apart from intrasite and intersite Coulomb repulsion interactions among the mobile e_g electrons, there are double exchange interaction between e_g spins,[50] electron−lattice interaction,[51] super-exchange interaction between the local spins,[52,53] and intersite exchange interaction between the e_g orbitals.[52,54]

Colossal magnetoresistance (CMR) manganites are well known for the large response of the electrical resistivity change to an external magnetic field.[55–57] The external magnetic field applied to the manganites plays a role through the double exchange (DE) interaction, which was first proposed by Zener in 1951 to explain[50] the strong correlation between ferromagnetism and metallic conductivity in doped manganites. This correlation can be well understood by the following formula proposed by Anderson and Hasegawa[58]:

$$t = t_0 \cos\left(\frac{\theta}{2}\right), \tag{4}$$

where t_0 is the normal transfer integral which depends on the spatial wavefunctions, θ is the angle between the two spin directions. As a naive explanation for the CMR effect, applying a magnetic field will turn the would-be insulating phase to metallic phase by aligning the spin directions.

Manganites provide a good playground for different interactions to compete with each other and reach delicate balance. Applying an external stimulus such as stress,[59–61] electromagnetic waves,[62] electrical field,[63,64] and so on can disturb this balance, and cause drastic changes in the physical properties such as electrical resistivity and magnetism. These properties make manganites very good candidate materials for constructing multifunctional nanodevices.

2.2. *AMR behaviors in perovskite manganites*

Many of the manganites possess cube like structure, and the AMR effect in these materials was deemed

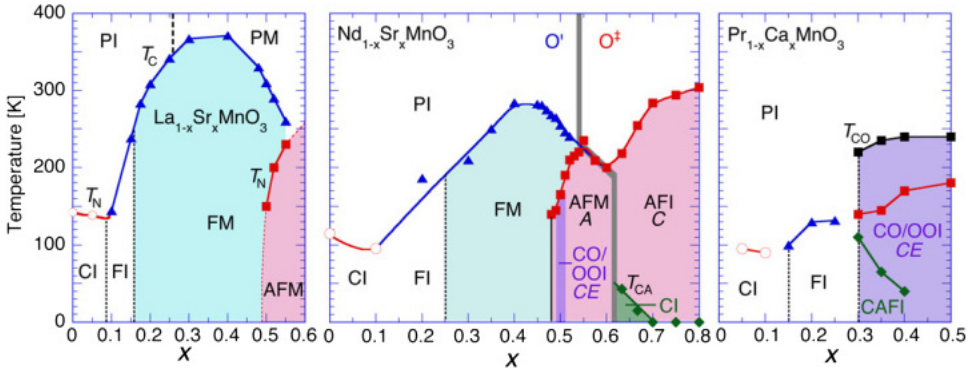

Fig. 4. Phase diagrams of some perovskite manganites. (Reproduced with permission from Ref. 55, Copyright 2006 IOP Publishing Ltd.).

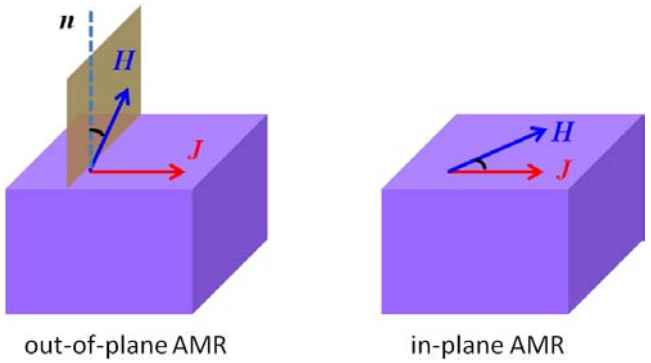

Fig. 5. Schematic picture showing the H–J configurations for measuring the out-of-plane and in-plane AMR effect.

to be small.[47,65] In 1996, Eckstein *et al.* reported[20] two-fold AMR curves in tetragonal $La_{1-x}Ca_xMnO_\delta$ thin films. Subsequent studies revealed[29,36,66] that the AMR effect in manganites shows different temperature — and magnetic field — dependence as compared with that of $3d$ ferromagnets, and the AMR magnitude can be comparable to that of the GMR and TMR value. Many extrinsic effects, including the substrate-induced strain and the large demagnetization field in the thin film geometry,[27,28,36] have been intensively investigated and found to greatly influence the anomalous AMR effect. AMR effects in manganites with different phases have also been conducted.

Experimentally, two kinds of **H**−**J** configurations have been adopted for assessing the AMR effect in perovskite manganites, which is schematically shown in Fig. 5. If the current **J** is kept fixed, and **H** is rotated in the plane that containing both **H** and **J**, we get the in-plane AMR. If **H** is perpendicular to **J** during a rotation, then we have out-of-plane AMR.

2.2.1. *AMR effect in ferromagnetic metallic manganites*

(1) $La_{1-x}Ca_xMnO_3$ (LCMO)

LCMO with $0.2 < x < 0.5$ owns orthorhombic structure and shows well-documented paramagnetic insulating to ferromagnetic metallic transition with lowering the temperature.[48] In $La_{0.69}Ca_{0.31}MnO_3$ single crystals, a strong temperature-dependent AMR has been demonstrated.[29] The AMR curves show two-fold symmetry and the peak value (as large as 90% at about 0.2 Tesla) is achieved very close to T_{MI} (∼220 K). There is no prominent AMR in the pure FM-metallic state and the pure

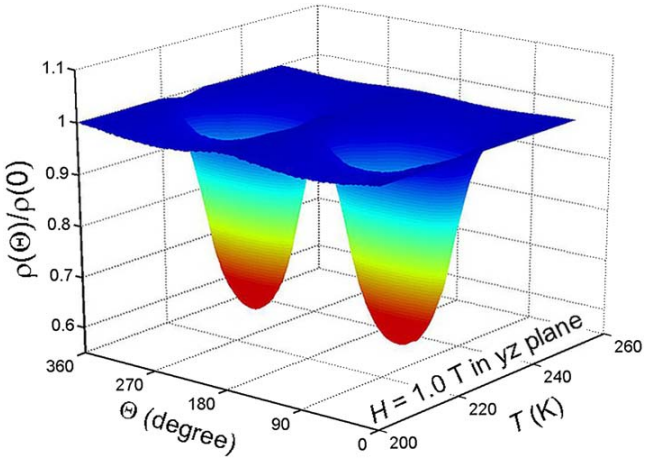

Fig. 6. Temperature dependences of the normalized out-of-plane AMR $\rho(\Theta)/\rho(\Theta = 0°)$ in $La_{0.69}Ca_{0.31}MnO_3$ single crystals, the applied magnetic field strength is 1.0 Tesla. (Reproduced with permission from Ref. 29.)

PM-insulating state, as shown in Fig. 6. At given temperature, the AMR shows nonmonotonic field-dependence, with a peak exists at certain magnetic field strength.

The temperature evolution of the AMR effect as well as its magnetic field dependence in manganites differs dramatically from what has been observed in conventional $3d$ ferromagnets, suggesting a different mechanism. Interestingly, there is a remarkable coincidence of the AMR peak value with the MIT (as shown in Fig. 7), manifesting a coherent coupling between them. In $La_{0.69}Ca_{0.31}MnO_3$ single crystals, the MR was found to have a strong dependence on lattice directions, which may originate from the cooperative JT distortions.

If the studied manganites are of polycrystalline form, where the crystalline anisotropy is averaged out, the AMR effect should be negligibly small. However, experimental results[45,67] show that the AMR effect in polycrystalline LCMO samples is not negligibly small, but shows a peak value near MIT. The AMR near MIT in polycrystalline LCMO samples is possibly caused by their phase separation nature,[45] where the metallic FM phase and insulating PM phase coexist. Under moderate magnetic field strength, the FM clusters tend to grow and elongated preferably along the external field direction, thus reaches a low resistance state when the magnetic field is parallel with current and high resistance state if the magnetic field is perpendicular to the current, this situation is schematically shown in Fig. 8.

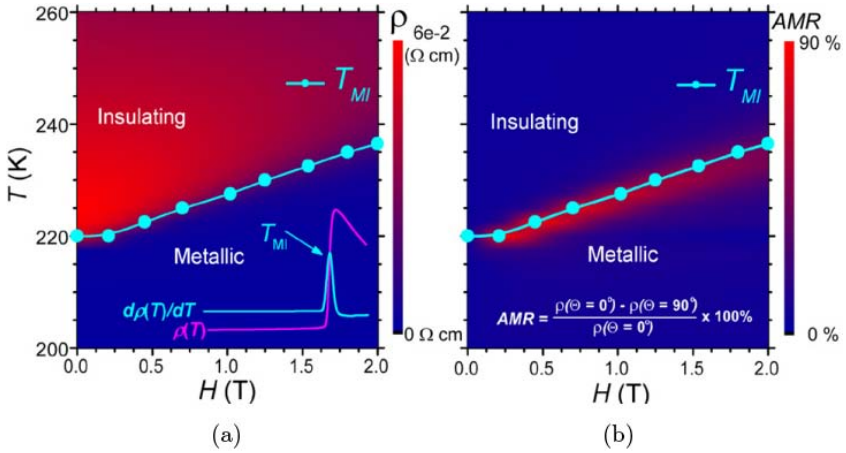

Fig. 7. Correlation between MIT and AMR in $La_{0.69}Ca_{0.31}MnO_3$ single crystals. (Reproduced with permission from Ref. 29.)

Intensive investigations have been devoted to study the AMR effect in perovskite manganite of thin film form, due to its potential for real applications. The AMR in perovskite manganites thin films generally follow that of the single crystalline form. For example, O'Donnell *et al.* reported[68] the AMR effect in $La_{0.7}Ca_{0.3}MnO_3$ thin films epitaxially grown on $SrTiO_3$ (001) substrates. They found that the magnitude of AMR is peaked near the Curie temperature and becomes small at low temperature. The AMR behaves very different from that in conventional metallic alloys, and also different from the low-field AMR.[69] The low-field AMR can show switching behavior that results from the jump of the magnetization from one easy axis to another,[70] but in their measurements, the applied magnetic fields are sufficiently larger than the coercive and anisotropy fields so that the magnetization rotates with the field. They attributed[71] the AMR effect to the SO coupling induced orbital deformation, which can influence the hopping conduction process in manganites.

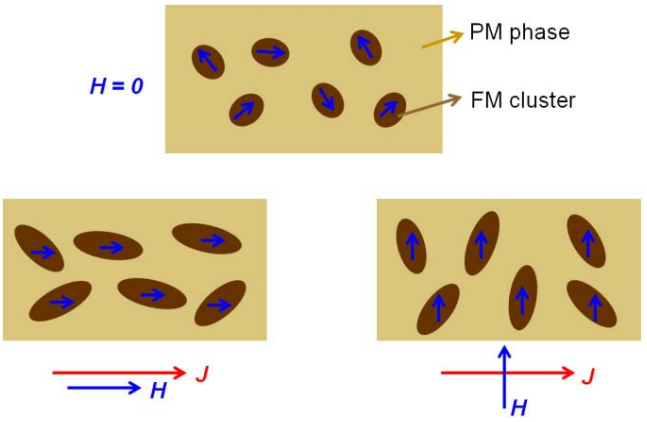

Fig. 8. Schematic picture for explaining the AMR effect near MIT in polycrystalline $La_{0.67}Ca_{0.33}MnO_3$ samples.

(2) $La_{1-x}Sr_xMnO_3$ (LSMO)

Bulk LSMO with $0.15 < x < 0.5$ possess rhombohedral structure and can exhibit MIT near room temperature. The AMR effect in LSMO has been studied mainly in thin film form. Yau *et al.* systematically studied[72] the AMR effect in LSMO epitaxial films as a function of temperature, magnetic field, and doping concentration, and two-fold in-plane AMR was found to show nonmonotonic dependence on temperature and magnetization (see in Fig. 9). Notice that the AMR value in LSMO is much lower than that in LCMO samples, which may be caused by the lattice mismatch effect.

Bibes *et al.* studied the AMR effect in $La_{0.67}Sr_{0.33}MnO_3$ thin films with different crystalline orientations.[73] They observed an AMR effect which shows uniaxial anisotropy at high magnetic field, but generally transforms into higher order symmetry at low field range as a result of the magnetocrystalline anisotropy. For example, in the (1 1 1) $La_{0.67}Sr_{0.33}MnO_3$ thin films, torque measurements under a magnetic field of 5 kOe revealed two-fold symmetry, which turns into four-fold with magnetic field lowered to 1 kOe. Consistently, they found that an intrinsic two-fold AMR curve is dominant for fields down to about 2 kOe, whereas at lower fields two small peaks start to develop coming from the four-fold dependence related to the anisotropy of the magnetization, as is shown in Fig. 10.

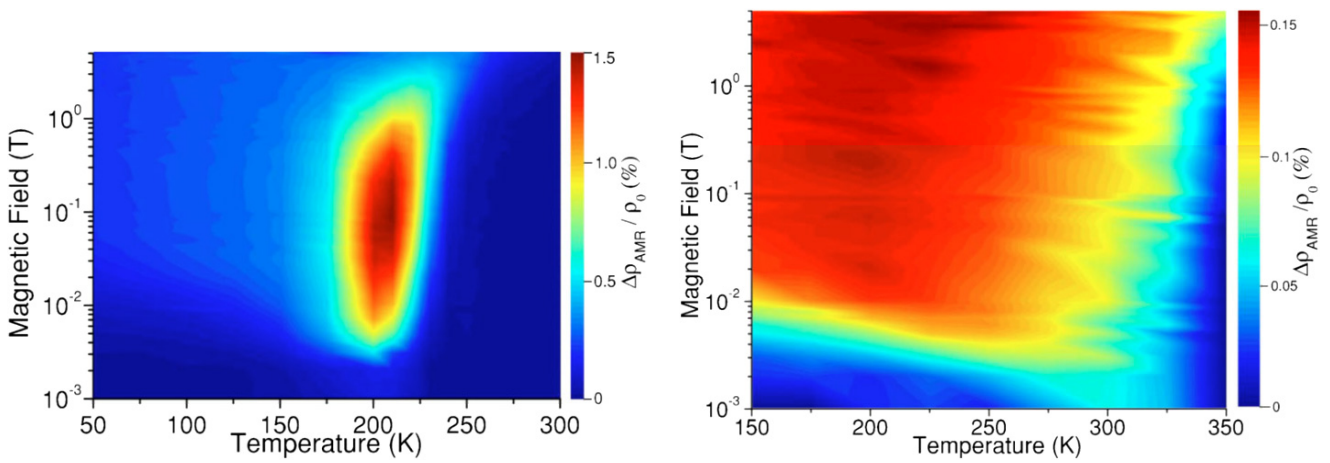

Fig. 9. $\Delta\rho_{AMR}/\rho_0$ measured as a function of temperature and magnetic field in (a) $x = 0.16$ LSMO and (b) $x = 0.35$ LSMO. (Reproduced with permission from Ref. 72, Copyright © 2007 American Institute of Physics.)

(3) $La_{1.2}Sr_{1.8}Mn_2O_7$

The $La_{2-2x}Sr_{1+2x}Mn_2O_7$ crystal possesses a quasi-two-dimensional structure, where the MnO_2 bilayers, separated by the insulating nonmagnetic (La, Sr)$_2O_2$ layers, are stacked along the c-axis. This reduced dimensionality leads to a strong crystalline anisotropy and anisotropic magneto-transportation behavior, thus large AMR effect was expected. The bilayered $La_{1.2}Sr_{1.8}Mn_2O_7$ single crystals show well-defined MIT behavior, as depicted in Fig. 11. A giant AMR was found[43] by rotating the magnetic field from c-axis to the $a-b$ plane, reaching a value of 80% under a magnetic field of 1.0 Tesla near the metal−insulator transition temperature. The AMR effect shows a close interrelation with the anisotropic field-tuned metal−insulator transition, and was attributed to the anisotropic lattice strain tuned by magnetic field in this layered system.

(4) $Pr_{0.67}Sr_{0.33}MnO_3$

In $Pr_{0.67}Sr_{0.33}MnO_3$ thin films, Li *et al.* reported[27] an anomalous AMR effect which was extremely sensitive to the epitaxial strain. The strain effect on AMR will be addressed in more detail later.

As can be seen from the above description, in manganites showing MIT phase transition, the

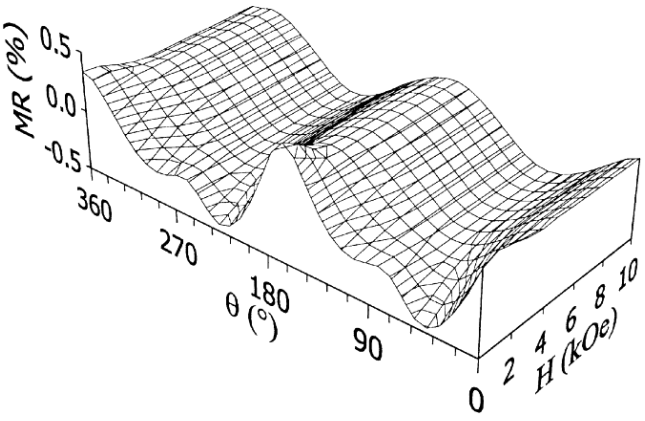

Fig. 10. Field dependence of the AMR curves for (1 1 1) $La_{0.67}Sr_{0.33}MnO_3$ at 10 K. (Reproduced with permission from Ref. 73, Copyright © 2000 Elsevier Science B.V.)

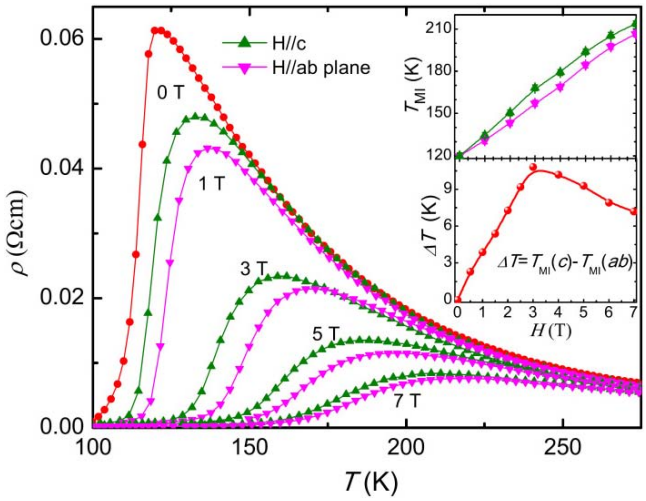

Fig. 11. Temperature dependence of the resistivity of bilayered $La_{1.2}Sr_{1.8}Mn_2O_7$ with magnetic fields applied along c-axis and in the $a-b$ plane. The upper inset presents the T_{MI} measured along two directions. The lower inset shows the difference ΔT_{MI} of T_{MI} along two directions. (Reproduced with permission from Ref. 43, Copyright © 2010 American Institute of Physics.)

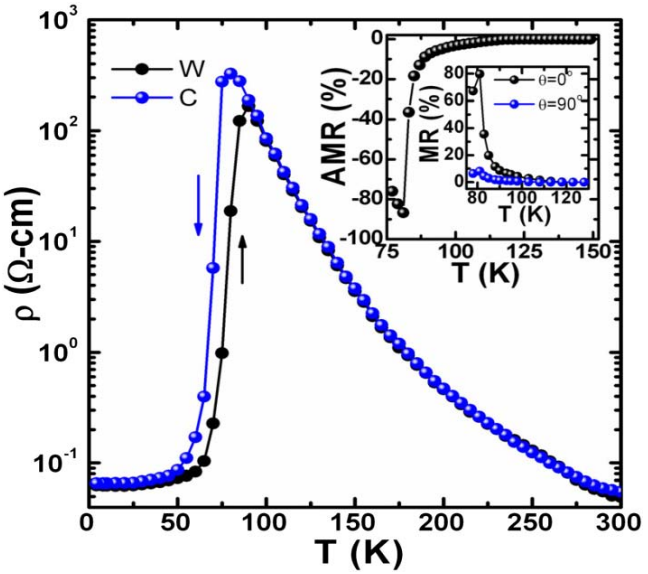

Fig. 12. Temperature-dependent resistivity of $Sm_{0.53}Sr_{0.47}MnO_3$ thin film measured in cooling and heating cycles. Inset shows the variation of AMR and MR with temperature when J is parallel to H ($\theta = 0°$) and perpendicular to it ($\theta = 90°$), the applied magnetic field is 3.6 KOe. (Reproduced with permission from Ref. 74, Copyright © 2011 American Institute of Physics.)

AMR amplitude all show their peaks near MIT, manifesting some universal mechanism underlying this phenomenon. There are also reports about the AMR effect in some manganites showing phase fluctuations near the MIT, such as $Sm_{0.53}Sr_{0.47}MnO_3$ (SSMO)[74] which lies near the boundary of FMM phase and CO-AFI phase.[75] Srivastava *et al.* reported that in SSMO thin films,[74] the coexistence of FMM phase and CO-AFI phase may induces hysteresis behavior in the isothermal magnetoresistivity. They also observed huge out-of-plane AMR effect near the MIT, which can reach a value of ∼88% at 78 K under a small magnetic field of 3.6 KOe, as shown in Fig. 12.

2.2.2. *AMR effect in antiferromagnetic insulating manganites*

(1) $La_{0.67}Ca_{0.33}MnO_3$

The observation of strong AMR effect was also reported[76] by Wang *et al.* in $La_{0.67}Ca_{0.33}MnO_3$ films grown coherently on the orthorhombic $NdGaO_3$ (001) substrates. Due to the pseudomorphic strain, the LCMO thin films show not only MIT near 265 K but also the coexistence of ferromagnetic metallic phase and antiferromagnetic insulating (AFI) phase

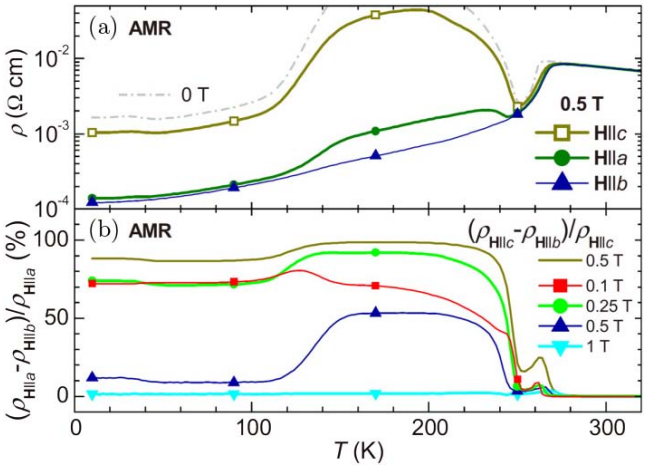

Fig. 13. (a) $\rho - T$ curve of $La_{0.67}Ca_{0.33}MnO_3$ films on FW at 0.5 T with H along a-, b-, and c-axes, respectively, and (b) the temperature-dependent in-plane AMR at 0.1, 0.25, 0.5, and 1 T, and out-of-plane AMR at 0.5 T. (Reproduced with permission from Ref. 76, Copyright © 2010 American Institute of Physics.)

below 250 K. They found that the phase competitions were very sensitive to the magnetic field and to its orientation with respect to the crystal axes, resulted in very large in-plane and out-of-plane AMR over a wide temperature range, as shown in Fig. 13.

They also found that by rotating the applied magnetic field, irreversible suppression of the AFI phase can be induced and very unique AMR curves exist, as shown in Fig. 14. Their results showed that the AMR effect is strongly coupled with the phase competition, and the SO coupling should play a significant role in explaining the AMR effect in manganites.

(2) $Pr_{0.7}Ca_{0.3}MnO_3$

The irreversible resistance drop in the AMR curves can also be observed in $Pr_{0.7}Ca_{0.3}MnO_3$ thin films, as

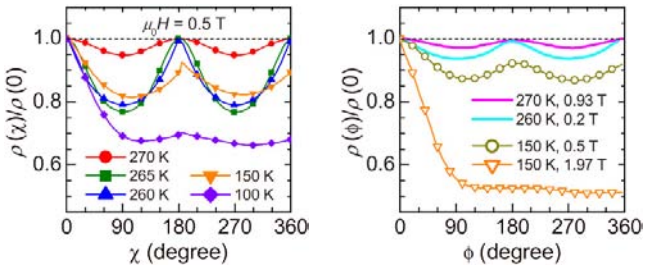

(a) (b)

Fig. 14. (a) Out-of-plane and (b) in-plane AMR curves of $La_{0.67}Ca_{0.33}MnO_3$ films measured at different T and H, as denoted. (Reproduced with permission from Ref. 76, Copyright © 2010 American Institute of Physics.)

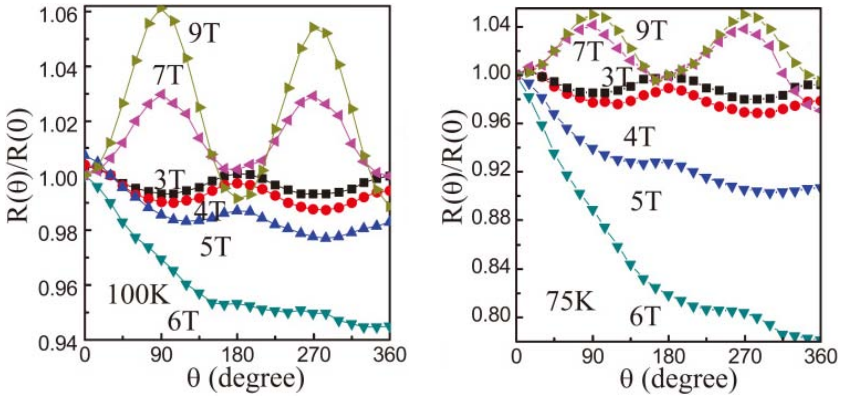

Fig. 15. Angular-dependent MR of $Pr_{0.7}Ca_{0.3}MnO_3$ thin films at (a) 100 K and (b) 75 K under different magnetic field strengths. (Reproduced with permission from Ref. 77, Copyright © 2011 American Institute of Physics.)

has been reported by Zhang *et al.*[77] As their prepared $Pr_{0.7}Ca_{0.3}MnO_3$ thin films show coexistence of FM phase and CO-AFI phase in the investigated temperature range, these unique AMR curves indicate the expanse of FM phase at the expense of CO-AFI phase. With the increase of applied magnetic field, they also observed a transition between $\cos^2\theta$-dependent AMR in an insulating state and $\sin^2\theta$-dependent AMR in a metal state, as shown in Fig. 15. They attributed this sign evolution of AMR to the magnetic field induced ferromagnetic metal percolation behavior.

(3) $Sm_{0.5}Ca_{0.5}MnO_3$

Chen *et al.* studied the in-plane AMR effect in charge-orbital ordered (COO) $Sm_{0.5}Ca_{0.5}MnO_3$ (SCMO) thin films,[78] which were grown on (0 1 1)-oriented $SrTiO_3$ substrates. The temperature and magnetic field dependence of the AMR effect with current along two orthogonal directions (1 0 0) and (0 −1 1) was studied. They observed a dramatic decrease of the AMR magnitude in both directions with the appearance of magnetic field induced MIT, which further led to a sign crossover in the AMR effect, as shown in Fig. 16. The sign changes indicate an opposite AMR behavior between the COO state and the field-induced metallic phase, which was suggested to be caused by the orbital reconstruction accompanying the magnetic field induced MIT.

(4) $Nd_{1-x}Sr_xMnO_3$ (NSMO)

The same group also investigated[79] the in-plane AMR effect in the (110)-oriented $Nd_{0.48}Sr_{0.52}MnO_3$ thin films, which show an orbital ordered AFM transition below $T_N \sim 203$ K. Accompanying the orbital ordering, they observed a significant enhancement of the AMR with current along the [1 0 0] direction and the appearance of four-fold symmetry of the AMR when the current is along the [1 −1 0] direction, as shown in Fig. 17. From

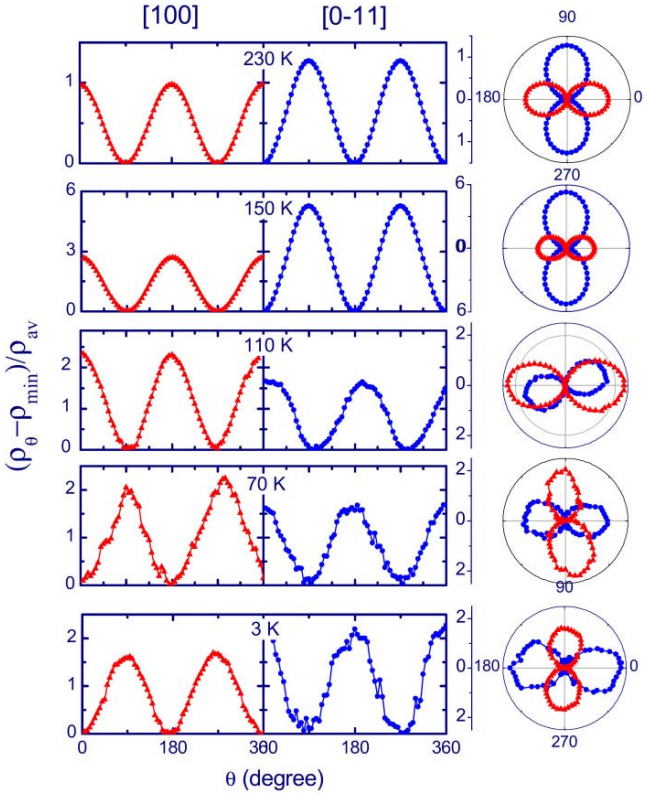

Fig. 16. Linear (left) and polar (right) plots of temperature-dependent evolution of AMR oscillations of $Sm_{0.5}Ca_{0.5}MnO_3$ (011) films along both [100] and [01−1] directions under a field of 13 T. (Reproduced with permission from Ref. 78, Copyright © 2009 American Institute of Physics.)

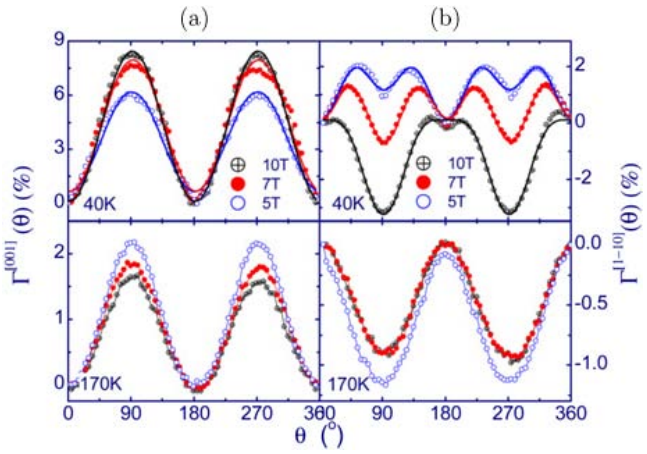

Fig. 17. Angular dependence of the magnetoresistance of the (110)-oriented $Nd_{0.48}Sr_{0.52}MnO_3$ thin films measured under different magnetic fields, with the current applied in the [001] and [1−10] direction, respectively. (Reproduced with permission from Ref. 79, Copyright © 2011 American Institute of Physics.)

symmetry consideration, this indicates that the transportation properties are different with current along the [1 0 0] and [1 −1 0] directions, which may result from the different strain state caused by the substrate.

The AMR effect in orbital ordered A-type AFM state have also been reported by Zhang *et al.* in $Nd_{0.45}Sr_{0.55}MnO_3$ (0 0 1) thin films,[80] where evolution between two-fold and four-fold symmetric AMR curves was discussed. The out-of-plane AMR exhibits two-fold symmetry at low magnetic fields and temperature region, and evolves into four-fold symmetry with increasing the magnetic field strength and temperatures, as can be seen in Fig. 18. However, for the in-plane AMR, higher temperature and larger magnetic field seems to favor two-fold symmetry behavior, and four-fold symmetry was

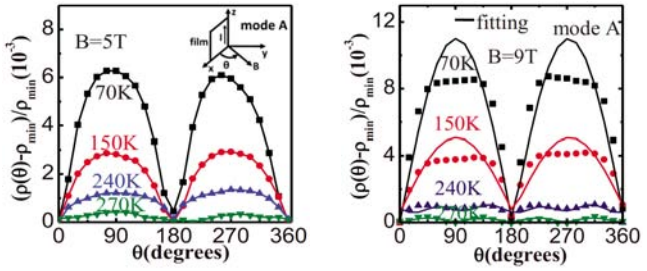

Fig. 18. Out-of-plane AMR of $Nd_{0.45}Sr_{0.55}MnO_3$ thin films at 270 K, 240 K, 150 K, and 70 K under magnetic fields of (a) 5 T and (b) 9 T, respectively. (Reproduced with permission from Ref. 80, Copyright © 2010 American Institute of Physics.)

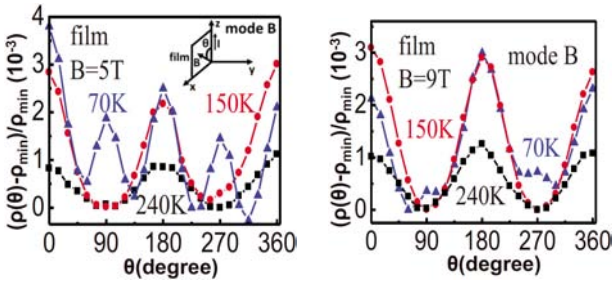

Fig. 19. In-plane AMR of the $Nd_{0.45}Sr_{0.55}MnO_3$ thin films at 240 K, 150 K, and 70 K under magnetic fields of (a) 5 T and (b) 9 T, respectively. (Reproduced with permission from Ref. 80, Copyright © 2010 American Institute of Physics.)

found at lower temperatures and magnetic fields, as shown in Fig. 19. This symmetry evolution was suggested to originate from the magnetic-field induced spin-canting states based on the A-type AFM structure.

2.3. *Tuning the AMR effects in manganites*

As have been addressed before, the versatile physical properties exhibited by manganites are very sensitive to external stimulus such as chemical doping, stress state, electrical field and electromagnetic radiation. In order to make use of the AMR effect in manganites, it is necessary to study the effect of external stimulus on the AMR properties.

2.3.1. *Chemical doping effects*

Doping is a very useful way for the investigation of phase evolution in perovskite manganites, since doping can usefully tune the lattice distortion as well as the band filling. Lattice distortion can cause the bending of the Mn−O−Mn bond, which may cause reduction of the effective *d*-electron transfer amplitude *t* between the neighboring Mn sites which is governed by the *d*-electron hybridization with the intervening O 2*p* state.

As have been introduced above, $La_{0.67}Ca_{0.33}MnO_3$ have a much higher AMR value than that of $La_{0.67}Sr_{0.33}MnO_3$, it seems we can get sizable AMR value at room temperature by doping moderate Sr element into $La_{0.67}Ca_{0.33}MnO_3$. However, this attempt failed because the AMR value of $La_{0.67}Ca_{0.33}MnO_3$ drops steeply with the addition of Sr element, as is shown in Fig. 20. We can only get

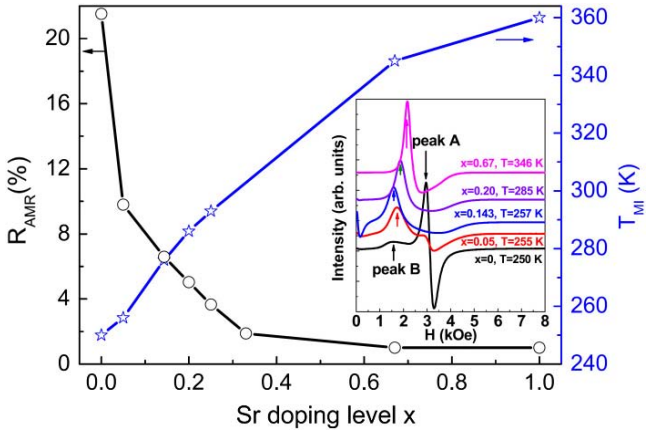

Fig. 20. AMR and T_{MI} for $La_{0.67}(Ca,Sr)_{0.33}MnO_3$ as a function of Sr content (x). The inset shows the ESR spectra for $La_{0.67}(Ca,Sr)_{0.33}MnO_3$ with various Sr content x near T_{MI}. (Reproduced with permission from Ref. 45, Copyright 2012 IOP Publishing Ltd.)

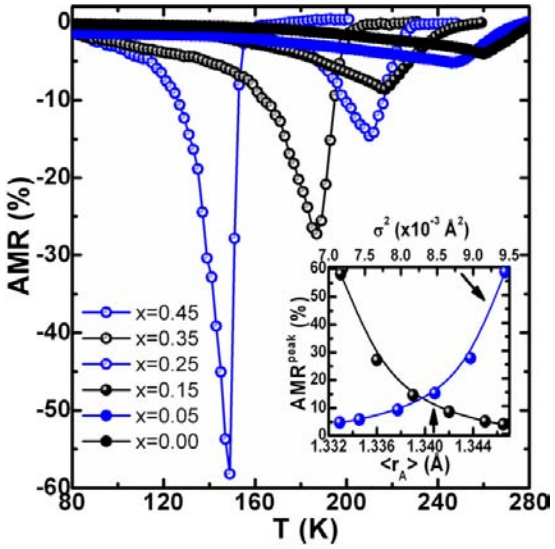

Fig. 21. Variation of AMR with temperature of the $Nd_{0.55-x}Sm_xSr_{0.45}MnO_3$ ($x = 0.0-0.45$) thin films. Inset shows the variation of AMR peak with the A-site radii $\langle r_A \rangle$ and the size disorder σ^2. (Reproduced with permission from Ref. 44, Copyright © 2012 American Institute of Physics.)

an AMR value of about 3% at room temperature with substituting 33% of Ca ions, even though $La_{0.67}Ca_{0.33}MnO_3$ shows about 20% AMR value near 250 K. Electron Spin Resonance (ESR) spectra (as shown in the inset of Fig. 20) show rapid vanishing of the phase coexistence with Sr doping, indicating that phase fluctuation also plays significant role in determining the AMR value.

The AMR effect in $Nd_{0.55-x}Sm_xSr_{0.45}MnO_3$ ($x = 0.0-0.45$) thin films[44] has been investigated with the aim to study the impact of lattice distortion on it. By substituting smaller Sm^{3+} cations for larger Nd^{3+} will cause a reduction of the average radius in the A-site and enhance the size disorder, thus induce an enhanced JT distortion. This distortion strengthens the carrier localization by enhancing the activation energy of small polaron hopping, which is evidenced by the decrease of T_{MI} and an enhanced MR effect. Accompanying with the enhanced JT distortion and phase fluctuation, they observed a large enhancement in the AMR value, which is summarized in Fig. 21.

2.3.2. *Strain control of AMR effect*

The strain effect on AMR in manganite thin films has been systematically studied through different ways. One way is by using the strain caused by the lattice mismatch between substrates and the epitaxially grown thin films. Choosing a substrate with lattice constant larger than that of the thin film (for example, LCMO grown on $SrTiO_3$) will cause tensile strain of the film, and substrate with lattice constant smaller than that of the thin film (for example, LCMO grown on $LaAlO_3$) will cause compressive strain. The epitaxial strain will decay with growing of film thickness, and the strain is relieved by defects such as dislocation in order to minimize the energy. The AMR effect near T_{MI} in strained films of $La_{0.65}Ca_{0.35}MnO_3$ (epitaxially grown on LAO substrates) as a function of the film thickness has been investigated.[81] The authors found that reducing the film thickness can greatly enhance the in-plane AMR. As a result, increase in the epitaxial lattice strain can promote the AMR value. The same group also studied the epitaxial strain effect by comparing the AMR effect between ultra-thin LCMO thin films that were grown simultaneously on STO and LAO substrates in order to avoid any differences in the deposition conditions.[28] For both films deposited on STO and LAO substrate, they found an enhancement in the AMR value with decreasing the film thickness, as is shown in Fig. 22. At temperatures far below MIT, the AMR in ultra-thin LCMO films on LAO changes sign with increasing magnetic field, which is not observed in LCMO films on STO, as depicted in Fig. 23. From these results, we can see that the epitaxial strain can affect the AMR in a very complex way and there is still no theoretical treatment of this phenomenon.

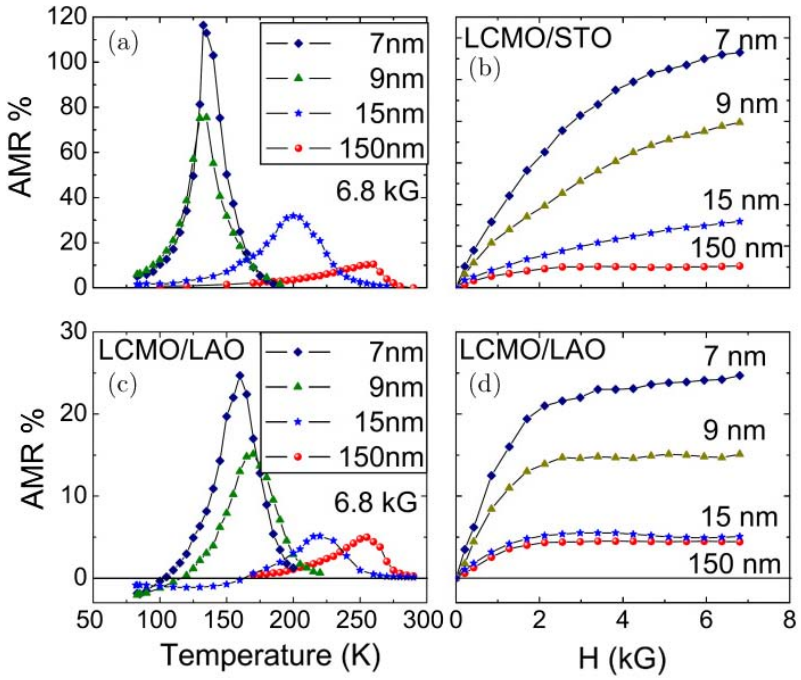

Fig. 22. [(a) and (c)] Temperature dependence of the AMR in the $La_{0.65}Ca_{0.35}MnO_3$ (LCMO)/$SrTiO_3$ (STO) and LCMO/$LaAlO_3$ (LAO) films measured in a field of 6.8 Kg. [(b) and (d)] The field dependence of the AMR in the LCMO/STO and LCMO/LAO films measured at the AMR peak's maximum. (Reproduced with permission from Ref. 28, Copyright © 2008 American Institute of Physics.)

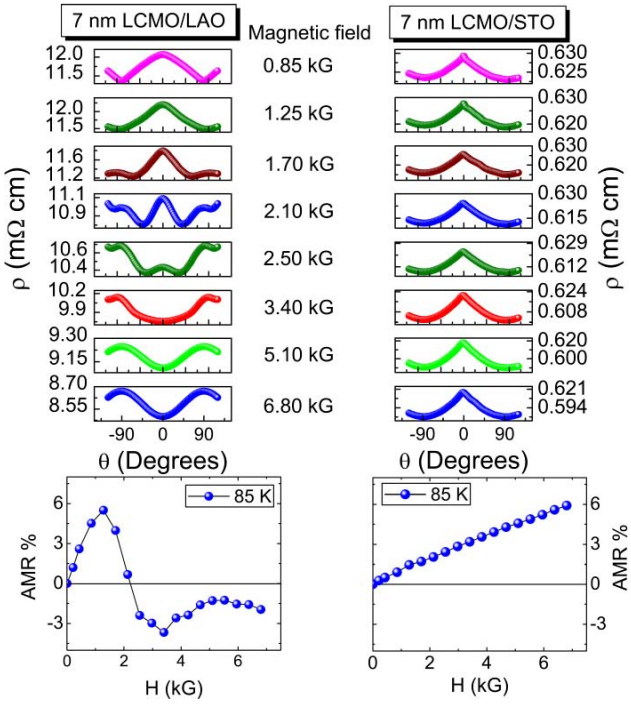

Fig. 23. (Upper panel) Angular-dependent magneto-resistivity measured at 85 K for the 7 nm thick $La_{0.65}Ca_{0.35}MnO_3$ (LCMO)/LAO and LCMO/STO films. (Lower panel) Corresponding dependence of AMR on the applied magnetic field. (Reproduced with permission from Ref. 28, Copyright © 2008 American Institute of Physics.)

The strain effect on AMR of $Pr_{0.67}Sr_{0.33}MnO_3$ (PSMO) thin films has been systematically investigated by Li's group. They grow the PSMO thin films epitaxially on different substrates, and obtained compressive (on LAO), tensile (on STO), and nearly free strain (on NGO) in the films.[27] The out-of-plane AMR was measured at a fixed temperature, with the applied magnetic field large enough to fully saturate the films,[82] so that the shape demagnetization effect is negligibly small. Their results showed unusually large AMR at both compressive- and tensile-strained ultrathin films (50−150 Å), but with opposite signs, as is shown in Figs. 24 and 25. In contrast, they found a much smaller AMR in the almost strain free films over all the studied temperature and field ranges. Consistently, the AMR value decreased rapidly as the film thickness increased due to the gradual release of strain.

Investigation of the strain effect on AMR was also conducted on epitaxially grown manganite thin films on piezoelectric substrates. By applying electric field to piezoelectric substrates, we can trig lattice deformation which may transmit into the thin films deposited on the substrates. In this way, it is possible to study the strain effect on AMR in a tunable way. Li's group[83] studied the strain effect on

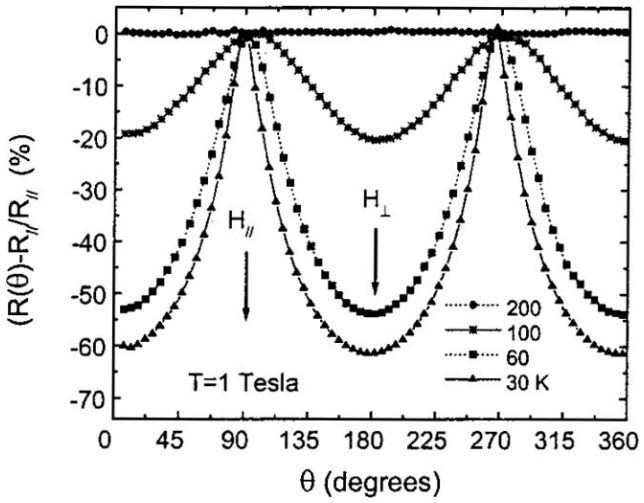

(a)

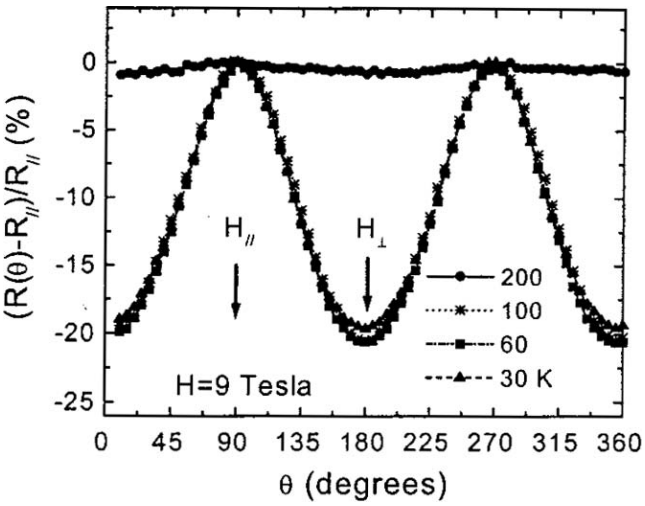

(b)

Fig. 24. The $[R(\theta) - R_{\|}]/R_{\|}$ versus θ curves for a 5-nm-thick $Pr_{0.67}Sr_{0.33}MnO_3/LaAlO_3$ film measured at different temperatures and at $H = 1\,T$ (a), and $H = 9\,T$ (b), respectively. (Reproduced with permission from Ref. 82, Copyright © 2000 American Institute of Physics.)

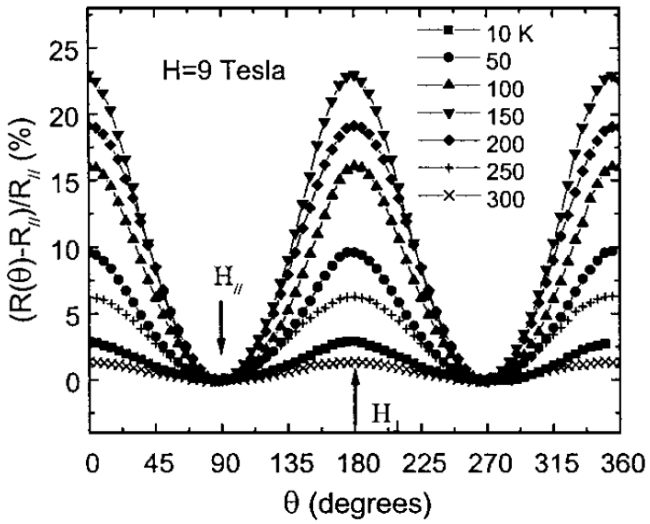

Fig. 25. The $[R(\theta) - R_{\|}]/_{R\|}$ versus θ curves for a 15-nm-thick $Pr_{0.67}Sr_{0.33}MnO_3/SrTiO_3$ film measured at different temperatures with $H = 9\,T$. (Reproduced with permission from Ref. 82, Copyright © 2000 American Institute of Physics.)

AMR in LCMO thin films by depositing them on ferroelectric $BaTiO_3$ (BTO) substrates. The BTO substrates will go through a series of structural phase transitions with varying temperatures, and the lattice deformations induced by the phase transition will be efficiently transferred to the LCMO thin films, thus enable a systematical study of the strain on the AMR effect on manganites thin films. They found that for very thin films (less than 80 nm) deposited on BTO substrates, the AMR amplitude increases with lowering the temperature. This makes drastic contrast with that of thicker films, where peak AMR values can be observed near T_{MI}. For the 80 nm LCMO films on BTO, they also observed the sign flips of AMR with a change of the strain state at different BTO phases, suggesting dramatic modification of the AMR effect can be induced by the epitaxial strain.

2.3.3. *Electrical modulation of AMR effects*

Besides strain modulation, electric field is another very important parameter for controlling the physical properties of manganites. Applying an electric field can modulate the carrier concentration, which may shift the subtle balance between phase competitions and possibly tune the AMR effect. In order to induce significant changes of the charge carriers, an electric field comparable to the areal carrier density of the system should be required, which constructs severe challenges in manganites, where the heavy carrier concentration (for example, a carrier density in the order of 10^{21} per cm^3 has been revealed in the metallic state of $La_{1-x}Sr_xMnO_3$) generally results in an electronic screening length of about only one atomic layer.[84] In order to study the effect of electric field modulation on the AMR effect in manganites, LSMO films with a thickness of 3 nm has been deposited on ferroelectric $Pb(Zr_{0.2}Ti_{0.8})O_3$ (PZT). By Hall effect measurements,[85] the authors estimated carrier densities of ~ 0.3 carriers per unit cell in the accumulation state and ~ 0.2 carriers per unit

cell in the depletion state. They measured the electric modulation of AMR in LSMO thin films with $x = 0.33$, 0.2, and 0.16, and $La_{1-x}Ca_xMnO_3$ thin films with $x = 0.3$, and found that while the electric field doping can significantly modulate the magnetic Curie temperature and resistivity of manganite thin films, its tuning on AMR effect is negligible. This makes sharp contrast with chemical doping experiments, where modulation of the carrier concentration by 0.1 per unit cell changes the AMR ratio by more than 30%. The difference between electric modulation and chemical doping is summarized in Fig. 26, from which a dominant role of chemical doping induced lattice distortion in determining the AMR in manganites is revealed.

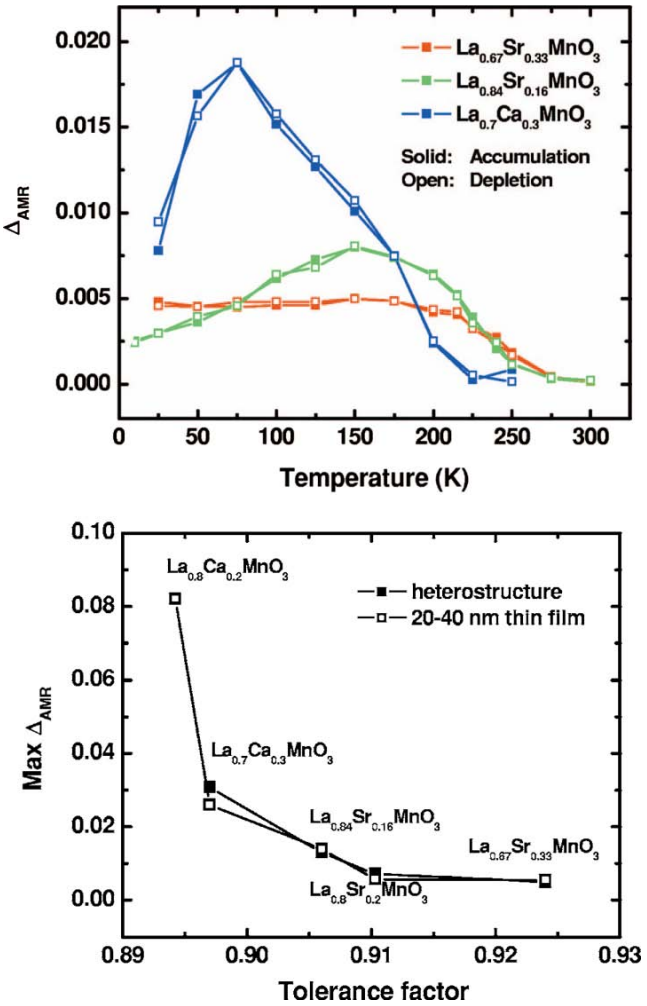

Fig. 26. Upper panel: temperature dependence of AMR at 7 kOe for accumulation (solid) and depletion (open) states taken on LSMO heterostructures with $x = 0.33$ (red) and 0.16 (green), and $La_{0.7}Ca_{0.3}MnO_3$ heterostructure (blue); Lower panel: Maximum AMR measured as a function of the tolerance factor for LSMO and LCMO heterostructures (solid) and single layer films (open). (Reproduced with permission from Ref. 85, Copyright © 2006 The American Physical Society.)

2.4. *Mechanisms of AMR effects in perovskite manganites*

Up to now, intensive studies have been conducted on the AMR effect in $3d$ ferromagnets, and much has been gained about the transportation properties in these materials.[7,86,87] Based on Mott's two current model,[10] Smit proposed[11] that the AMR effect in $3d$ ferromagnets comes from the SO coupling effect:

$$H_{SO} = \lambda\left[L_Z S_Z + \frac{1}{2}(L_+ S_- + L_- S_+)\right], \quad (5)$$

where λ is the SO coupling constant, the z components and climbing operators of the spin S and angular momentum L are defined in the usual way. According to the two-current model, the s electrons with two spin state (spin $_\uparrow$ and spin $_\downarrow$) constitute two parallel conduction channels with resistivity of $\rho_\uparrow$ and $\rho_\downarrow$, respectively. Taken spin-flip process (assigned with resistivity $\rho_{\uparrow\downarrow}$) into account, the total resistivity can be expressed by the following formula[7]:

$$\rho = \frac{\rho_\uparrow\rho_\downarrow + \rho_{\uparrow\downarrow}(\rho_\uparrow + \rho_\downarrow)}{\rho_\uparrow + \rho_\downarrow + 4\rho_{\uparrow\downarrow}}. \quad (6)$$

For each spin current, the resistivity comes from the dominated $s-d$ and the minor $s-s$ scattering process, which can be expressed as $\rho_\sigma = \rho_{s\sigma} + \rho_{s\sigma\to d\mu}$ (where σ and μ denote the spin state of s and d electrons, respectively). As a result of the SO coupling, the d orbitals are unevenly mixed, thus the resistivity $\rho_{s\sigma\to d\mu}$ becomes dependent on the magnetic field direction,[88] causing the AMR effect. Take $\Delta\rho_\downarrow$ and $\Delta\rho_\uparrow$ to denote the resistivity changes between $\mathbf{M}\|\mathbf{J}$ and $\mathbf{M}\perp\mathbf{J}$ of the spin $_\uparrow$ and spin $_\downarrow$ channels, then we have the general expression[86]:

$$\begin{aligned}\Delta\rho_\uparrow &= \gamma_{\uparrow\uparrow}\rho_\uparrow + \gamma_{\uparrow\downarrow}\rho_\downarrow \\ \Delta\rho_\downarrow &= \gamma_{\downarrow\uparrow}\rho_\uparrow + \gamma_{\downarrow\downarrow}\rho_\downarrow\end{aligned}. \quad (7)$$

In the case of strong ferromagnets, such as some dilute Ni alloys, $\rho_\downarrow \gg \rho_\uparrow$, therefore Eq. (7) is reduced to $\Delta\rho_\downarrow = -\gamma\rho_\downarrow$ and $\Delta\rho_\uparrow = \gamma\rho_\downarrow$. Neglect the spin-flip scattering, and the well-known results of Campbell *et al.*[88] is obtained as:

$$\frac{\Delta\rho}{\rho} = \gamma(\alpha - 1), \quad (8)$$

where $\alpha = \rho_\downarrow/\rho_\uparrow$ and γ is proportional to the SO coupling constant λ. A more realistic analysis by including the cubic anisotropy has been made by Malozemoff.[86]

In perovskite manganites, the carriers are moving by hopping between the d states of the transition metal, thus needs modifications in describing the microscopic mechanism of AMR effect in perovskite manganites. Despite of this inconsistence, the AMR effect in double exchange manganites has been estimated based on the two-current SO coupling model,[42,89] where the itinerant d electrons are treated approximately as plane waves. For example, Ziese estimated[89] the AMR effect of $La_{0.7}Ca_{0.3}MnO_3$ based on the model proposed by Malozemoff, and found that the AMR value correspond well with only the majority electron conducting current and only a weak influence of a minority spin band exists.

A more realistic model was proposed by Fuhr *et al.*[90] based on the effect of SO coupling on the electronic structure, which can be regarded as the starting model for understanding the AMR effect in manganites. They modeled the itinerant e_g electrons by a spinless Hamiltonian on acubic lattice[91]:

$$H = \sum_{\langle ij\rangle\alpha\beta} t_{ij}^{\alpha\beta} c_{i\alpha}^{\dagger} c_{j\beta} \tag{9}$$

with $t_{ij}^{\alpha\beta}$ the hopping integrals that depend both on the type of orbitals (α, β) and on the direction between neighboring sites (i, j). The carrier transport properties were obtained by adopting the transport formula for Fermi quasi-particles, based on which the conductivity tensor components σ_{ij} can be expressed as:

$$\sigma_{ij} = e^2\tau \sum_n \int d^3k \frac{\partial f}{\partial \varepsilon_n(\mathbf{k})} \frac{\partial \varepsilon_n(\mathbf{k})}{\partial k_i} \frac{\partial \varepsilon_n(\mathbf{k})}{\partial k_j} \tag{10}$$

with the relaxation time τ assumed to be isotropic, and $f\ (\varepsilon)$ denoting the Fermi function. The band dispersion $\varepsilon_n(\mathbf{k})$ is obtained by diagonalizing the total Hamiltonian $\mathbf{H}(\mathbf{k}) + \mathbf{H}_{\mathrm{SO}}$, where $\mathbf{H}(\mathbf{k})$ is the Fourier transform of Eq. (9), and $\mathbf{H}_{\mathrm{SO}}$ denotes the in-site SO coupling. The SO coupling can lift the degeneracy of the e_g orbitals, and cause the shift and coupling of the two original e_g orbitals depending on the magnetization ($\mathbf{M}$) direction, the SO coupling constant (λ), and the crystal field splitting (Δ_{CF}) between t_{2g} and e_g orbitals. They applied this model to the ferromagnetic manganite $La_{0.75}Sr_{0.25}MnO_3$ (LSMO) which represents a nearly cubic perovskite structure, and calculated ρ, for the case of magnetic field rotating in the (0 0 1) plane, as: $\rho = \rho_m[1 - A\cos(2\theta)\cos(2\beta)]$, where θ and β denote the angle of the current direction and the magnetic field direction with reference to the [100] direction of the film, respectively. Experimentally, they observed an AMR value of about 10^{-3} for the current I parallel to the [100] axis but vanishing AMR for I // [110], which is in agreement with the model predictions.

Just as the authors have stated, this simple model is just a starting point, and its extension to higher temperatures is far from straightforward. A complete understanding of the AMR requires incorporation of many other terms into calculations, where the spin−orbital−lattice coupling should be seriously considered. Li *et al.* systematically studied the AMR effect in $La_{0.69}Ca_{0.31}MnO_3$ single crystals[29] and found that the AMR effect in $La_{0.69}Ca_{0.31}MnO_3$ single crystal is caused by the crystalline orientation-dependent MIT behavior. As the orthorhombic structure of $La_{0.69}Ca_{0.31}MnO_3$ derivates from the cubic structure through the $a-b$ plane rotation and c-axis tilt of the MnO_6 octahedron, under the delicate interplay between JT distortions and DE interaction, the lattice may have different response with magnetic field applied perpendicular and parallel to the c-axis, causing the anomalous AMR effect. From the above analysis, we can see that the JT distortions should play a significant role in determining the AMR behavior. Based on this model, we can easily understand that $La_{0.67}Sr_{0.33}MnO_3$ has a smaller AMR effect than $Pr_{0.67}Sr_{0.33}MnO_3$ and $La_{0.67}Ca_{0.33}MnO_3$ because the former has smaller JT distortions. This also agrees with the fact that the AMR value of $SrRuO_3$ ferromagnetic oxide, where no JT distortion happens in Ru^{4+} ion, shows no enhancement near the Curie temperature.[92]

Another important factor influences the AMR effect of perovskite manganites is the strength of phase fluctuation. This can be seen from the result of Sr doping on the AMR effect of $La_{0.67}Ca_{0.33}MnO_3$ ceramics, and the evolution of AMR value by introducing Sm^{3+} ions in $Nd_{0.55}Sr_{0.45}MnO_3$ thin films. Manganites with stronger phase fluctuations are more sensitive to the external stimulus, thus we naturally expect a larger anisotropic magneto-transportation response. This effect can be understood more clearly by the rather similar material dependences of the CMR and AMR value.[70]

3. Conclusion and Outlooks

In summary, the AMR effect has attracted people's eyes for more than one century and is still a very hot topic in condense matter physics. Due to the strong spin−orbital−lattice coupling in perovskite manganites, a small crystalline anisotropy may result in a huge magneto-transport response and results in sizeable AMR effects that behave very differently as compared with that in $3d$ ferromagnets.

Although the AMR effect in perovskite manganites has triggered a wide range of interest, the mechanisms behind are far from clear. How is the spin coupled to the carriers' transportation? Is it possible to tune this coupling in an easy and controllable way? What is the effect of dimensionality on the AMR effect? These questions have to be answered if we want to make full utility of the novel AMR effect. Further studies corresponding to these questions should be carried out, as discussed below.

(1) The underlying physics for determining the AMR effect in manganites has to be further clarified. Although it has been suggested that the dissimilar JT effect as well as phase fluctuations play significant roles in explaining the anomalous AMR effect in ferromagnetic manganites, there is still no standard theoretic model. The critical factors for determining the AMR effect in other phases is not well understood. Even more, whether it is possible to give a unified explanation of the AMR in manganites is still a question.

(2) The AMR in low dimensional manganites structures has to be explored. Exploring novel effects in low-dimensional structures is a very attractive direction for the further shrinkage of electronic devices. With the advancement of material fabrication technology, preparing materials with various low dimensional structures becomes accessible. In order to prove the potential of hybrid low dimensional electronic-spintronic devices and the fundamental importance of spin phenomena at nanoscale, a number of studies of spin transport in low dimensional structures have been conducted, and very interesting phenomenon has been disclosed. As for the manganites, many studies have revealed the existence of the most fascinating phenomenon such as orbital reconstruction in ultra-thin films. How will the AMR effect look like when the dimensionality of perovskite manganites shrinks down? What will be the factors that influence the AMR effect in these low dimensional structures?

(3) Overcoming the open challenges in manganites-based devices. Manganites possess many interesting properties such as magnetic field sensitivity in electric transportation and half metallicity of the electronic structure, which would enable potential technological applications.[93] However, for real applications as MR sensors, there are still many challenges[93,94] such as: How to achieve large AMR value above room temperature under a small magnetic field? In what way can we improve the thermal stability of manganites-based devices, since the transportation properties of manganites shows strong temperature dependence? It has been reported[76] that in phase separated $La_{0.67}Ca_{0.33}MnO_3$ thin films, large AMR value may exists over a wide temperature range, so one possible way to get large AMR value above room temperature is by constructing artificial phase separated system.

Acknowledgment

The authors thank Dr. Sadhana Katlakunta for constructive discussions. This work was supported by National Natural Science Foundation of China (11274321), State Key Research Program of China (973 Program, 2009CB930803, 2012CB933004), Chinese Academy of Sciences (CAS), the Projects of Nonprofit Technology & Research in Zhejiang Province, and the Science and Technology Innovative Research Team of Ningbo Municipality (2009B21005, 2011B82004).

References

1. W. Thomson, *Proc. R. Soc. Lond.* **8**, 546 (1856).
2. T. R. McGuire and R. I. Potter, *IEEE Trans. Magn.* **11**, 1018 (1975).
3. T. McGuire, J. Aboaf and E. Klokholm, *IEEE Trans. Magn.* **20**, 972 (1984).
4. A. P. Malozemoff, *Phys. Rev. B* **32**, 6080 (1985).
5. T. G. S. M. Rijks, S. K. J. Lenczowski, R. Coehoorn and W. J. M. de Jonge, *Phys. Rev. B* **56**, 362 (1997).
6. M. Tsunoda, Y. Komasaki, S. Kokado, S. Isogami, C. C. Chen and M. Takahashi, *Appl. Phys. Express* **2**, 083001 (2009).
7. I. A. Campbell and A. Fert, *Handbook of Ferromagnetic Materials*, ed. E. P. Wohlfarth, Vol. 3 (Elsevier, 1982), pp. 747−804.

8. R. R. Birss, *Symmetry and Magnetism* (North-Holland Pub. Co., 1964).
9. C. M. Hurd, *Adv. Phys.* **23**, 315 (1974).
10. N. F. Mott, *Proc. R. Soc. Lond. A* **153**, 699 (1936).
11. J. Smit, *Physica* **17**, 612 (1951).
12. M. N. Baibich, J. M. Broto, A. Fert, F. N. Vandau, F. Petroff, P. Eitenne, G. Creuzet, A. Friederich and J. Chazelas, *Phys. Rev. Lett.* **61**, 2472 (1988).
13. G. Binasch, P. Grunberg, F. Saurenbach and W. Zinn, *Phys. Rev. B* **39**, 4828 (1989).
14. J. S. Moodera, L. R. Kinder, T. M. Wong and R. Meservey, *Phys. Rev. Lett.* **74**, 3273 (1995).
15. J. Velev, R. F. Sabirianov, S. S. Jaswal and E. Y. Tsymbal, *Phys. Rev. Lett.* **94**, 127203 (2005).
16. C. Rüster, C. Gould, T. Jungwirth, J. Sinova, G. M. Schott, R. Giraud, K. Brunner, G. Schmidt and L. W. Molenkamp, *Phys. Rev. Lett.* **94**, 027203 (2005).
17. J. Wunderlich, T. Jungwirth, B. Kaestner, A. C. Irvine, A. B. Shick, N. Stone, K. Y. Wang, U. Rana, A. D. Giddings, C. T. Foxon, R. P. Campion, D. A. Williams and B. L. Gallagher, *Phys. Rev. Lett.* **97**, 077201 (2006).
18. A. Bernand-Mantel, P. Seneor, K. Bouzehouane, S. Fusil, C. Deranlot, F. Petroff and A. Fert, *Nat. Phys.* **5**, 920 (2009).
19. Z.-M. Liao, H.-C. Wu, S. Kumar, G. S. Duesberg, Y.-B. Zhou, G. L. W. Cross, I. V. Shvets and D.-P. Yu, *Adv. Mater.* **24**, 1862 (2012).
20. J. N. Eckstein, I. Bozovic, J. Odonnell, M. Onellion and M. S. Rzchowski, *Appl. Phys. Lett.* **69**, 1312 (1996).
21. Z. J. Yue, X. L. Wang, Y. Du, S. M. Mahboobeh, F. Y. Frank, Z. X. Cheng and S. X. Dou, *Europhys. Lett.* **100**, 17014 (2012).
22. Q. Li, P. Ghosh, J. D. Sau, S. Tewari and S. Das Sarma, *Phys. Rev. B* **83**, 085110 (2011).
23. H. Tang, D. Liang, R. L. J. Qiu and X. P. A. Gao, *ACS Nano* **5**, 7510 (2011).
24. H. Sugawara, E. Kuramochi, T. Namiki, T. D. Matsuda, Y. Aoki and H. Sato, *J. Phys. Soc. Jpn.* **77**, 085001 (2008).
25. X. Su, F. Zuo, J. A. Schlueter, J. M. Williams, P. G. Nixon, R. W. Winter and G. L. Gard, *Phys. Rev. B* **59**, 4376 (1999).
26. J. Hua, Z. L. Xiao, A. Imre, S. H. Yu, U. Patel, L. E. Ocola, R. Divan, A. Koshelev, J. Pearson, U. Welp and W. K. Kwok, *Phys. Rev. Lett.* **101**, 077003 (2008).
27. Q. Li, H. S. Wang, Y. F. Hu and E. Wertz, *J. Appl. Phys.* **87**, 5573 (2000).
28. M. Egilmez, M. M. Saber, A. I. Mansour, R. Ma, K. H. Chow and J. Jung, *Appl. Phys. Lett.* **93**, 182505 (2008).
29. R. W. Li, H. B. Wang, X. W. Wang, X. Z. Yu, Y. Matsui, Z. H. Cheng, B. G. Shen, E. W. Plummer and J. D. Zhang, *Proc. Natl. Acad. Sci. U. S. A.* **106**, 14224 (2009).
30. A. Sokolov, C. Zhang, E. Y. Tsymbal, J. Redepenning and B. Doudin, *Nat. Nanotechnol.* **2**, 171 (2007).
31. F. Matsukura, M. Sawicki, T. Dietl, D. Chiba and H. Ohno, *Physica E: Low-dimens. Syst. Nanostruct.* **21**, 1032 (2004).
32. K. Výborný, J. Kučera, J. Sinova, A. W. Rushforth, B. L. Gallagher and T. Jungwirth, *Phys. Rev. B* **80**, 165204 (2009).
33. R. R. Gareev, A. Petukhov, M. Schlapps, J. Sadowski and W. Wegscheider, *Appl. Phys. Lett.* **96**, 052114 (2010).
34. G. F. Chen, Z. Li, J. Dong, G. Li, W. Z. Hu, X. D. Zhang, X. H. Song, P. Zheng, N. L. Wang and J. L. Luo, *Phys. Rev. B* **78**, 224512 (2008).
35. K. D. D. Rathnayaka, D. G. Naugle, B. K. Cho and P. C. Canfield, *Phys. Rev. B* **53**, 5688 (1996).
36. P. Kumar, R. Prasad, R. K. Dwivedi and H. K. Singh, *J. Magn. Magn. Mater.* **323**, 2564 (2011).
37. A. C. Masset, C. Michel, A. Maignan, M. Hervieu, O. Toulemonde, F. Studer, B. Raveau and J. Hejtmanek, *Phys. Rev. B* **62**, 166 (2000).
38. A. N. Lavrov, H. J. Kang, Y. Kurita, T. Suzuki, S. Komiya, J. W. Lynn, S. H. Lee, P. Dai and Y. Ando, *Phys. Rev. Lett.* **92**, 227003 (2004).
39. T. Wu, C. H. Wang, G. Wu, D. F. Fang, J. L. Luo, G. T. Liu and X. H. Chen, *J. Phys.: Condens. Matter* **20**, 275226 (2008).
40. R. Ramos, S. K. Arora and I. V. Shvets, *Phys. Rev. B* **78**, 214402 (2008).
41. R.-W. Li *et al.*, Unpublished.
42. M. Ziese and S. P. Sena, *J. Phys.: Condes. Matter* **10**, 2727 (1998).
43. W. Ning, Z. Qu, Y. Zou, L. Ling, L. Zhang, C. Xi, H. Du, R. Li and Y. Zhang, *Appl. Phys. Lett.* **98**, 212503 (2011).
44. M. K. Srivastava, A. Kaur and H. K. Singh, *Appl. Phys. Lett.* **100**, 222408 (2012).
45. Y. Liu, Z. Yang, H. Yang, T. Zou, Y. Xie, B. Chen, Y. Sun, Q. Zhan and R. W. Li, *J. Phys. D: Appl. Phys.* **45**, 245001 (2012).
46. Z. Jirák, S. Krupička, V. Nekvasil, E. Pollert, G. Villeneuve and F. Zounová, *J. Magn. Magn. Mater.* **15–18**, Part 1, 519 (1980).
47. A. Urushibara, Y. Moritomo, T. Arima, A. Asamitsu, G. Kido and Y. Tokura, *Phys. Rev. B* **51**, 14103 (1995).
48. P. Schiffer, A. P. Ramirez, W. Bao and S. W. Cheong, *Phys. Rev. Lett.* **75**, 3336 (1995).
49. C. Martin, A. Maignan, M. Hervieu and B. Raveau, *Phys. Rev. B* **60**, 12191 (1999).
50. C. Zener, *Phys. Rev.* **82**, 403 (1951).

51. A. J. Millis, P. B. Littlewood and B. I. Shraiman, *Phys. Rev. Lett.* **74**, 5144 (1995).
52. H. A. Kramers, *Physica* **1**, 182 (1934).
53. P. W. Anderson, *Phys. Rev.* **79**, 350 (1950).
54. I. K. Kliment and D. I. Khomskiĭ, *Sov. Phys. Usp.* **25**, 231 (1982).
55. S. Jin, T. H. Tiefel, M. McCormack, R. A. Fastnacht, R. Ramesh and L. H. Chen, *Science* **264**, 413 (1994).
56. H. Kawano, R. Kajimoto, H. Yoshizawa, Y. Tomioka, H. Kuwahara and Y. Tokura, *Phys. Rev. Lett.* **78**, 4253 (1997).
57. Y. Tomioka, A. Asamitsu, H. Kuwahara, Y. Moritomo and Y. Tokura, *Phys. Rev. B* **53**, R1689 (1996).
58. P. W. Anderson and H. Hasegawa, *Phys. Rev.* **100**, 675 (1955).
59. Z. Fang, I. V. Solovyev and K. Terakura, *Phys. Rev. Lett.* **84**, 3169 (2000).
60. Y. Ding, D. Haskel, Y.-C. Tseng, E. Kaneshita, M. van Veenendaal, J. F. Mitchell, S. V. Sinogeikin, V. Prakapenka and H.-K. Mao, *Phys. Rev. Lett.* **102**, 237201 (2009).
61. Y. Tokura, H. Kuwahara, Y. Moritomo, Y. Tomioka and A. Asamitsu, *Phys. Rev. Lett.* **76**, 3184 (1996).
62. K. Miyano, T. Tanaka, Y. Tomioka and Y. Tokura, *Phys. Rev. Lett.* **78**, 4257 (1997).
63. A. Asamitsu, Y. Tomioka, H. Kuwahara and Y. Tokura, *Nature* **388**, 50 (1997).
64. V. Ponnambalam, S. Parashar, A. R. Raju and C. N. R. Rao, *Appl. Phys. Lett.* **74**, 206 (1999).
65. S. Jin, T. H. Tiefel, M. McCormack, R. A. Fastnacht, R. Ramesh and L. H. Chen, *Science* **264**, 413 (1994).
66. H. S. Wang, Q. Li, K. Liu and C. L. Chien, *Appl. Phys. Lett.* **74**, 2212 (1999).
67. M. Egilmez, R. C. Ma, K. H. Chow and J. Jung, *J. Appl. Phys.* **105**(7), (2009).
68. J. Odonnell, M. Onellion, M. S. Rzchowski, J. N. Eckstein and I. Bozovic, *J. Appl. Phys.* **81**, 4961 (1997).
69. J. O'Donnell, M. Onellion, M. S. Rzchowski, J. N. Eckstein and I. Bozovic, *Phys. Rev. B* **55**, 5873 (1997).
70. M. Egilmez, K. H. Chow and J. A. Jung, *Mod. Phys. Lett. B* **25**, 697 (2011).
71. J. O'Donnell, J. N. Eckstein and M. S. Rzchowski, *Appl. Phys. Lett.* **76**, 218 (2000).
72. J. B. Yau, X. Hong, A. Posadas, C. H. Ahn, W. Gao, E. Altman, Y. Bason, L. Klein, M. Sidorov and Z. Krivokapic, *J. Appl. Phys.* **102**, 103901 (2007).
73. M. Bibes, B. Martínez, J. Fontcuberta, V. Trtik, C. Ferrater, F. Sánchez, M. Varela, R. Hiergeist and K. Steenbeck, *J. Magn. Magn. Mater.* **211**, 206 (2000).
74. M. K. Srivastava, M. P. Singh, A. Kaur, F. S. Razavi and H. K. Singh, *J. Appl. Phys.* **110**, 123922 (2011).
75. P. M. Martin, J. B. Sampsell and J. C. Garland, *Phys. Rev. B* **15**, 5598 (1977).
76. L. F. Wang, Z. Huang, X. L. Tan, P. F. Chen, B. W. Zhi, G. M. Li and W. B. Wu, *Appl. Phys. Lett.* **97**, 242507 (2010).
77. Y. Q. Zhang, H. Meng, X. W. Wang, J. J. Liu, J. Du and Z. D. Zhang, *Appl. Phys. Lett.* **99**, 252502 (2011).
78. Y. Z. Chen, J. R. Sun, T. Y. Zhao, J. Wang, Z. H. Wang, B. G. Shen and N. Pryds, *Appl. Phys. Lett.* **95**, 132506 (2009).
79. S. Liang, J. R. Sun, Y. Z. Chen and B. G. Shen, *J. Appl. Phys.* **110**, 96103 (2011).
80. Y. Q. Zhang, H. Meng, X. W. Wang, X. Wang, H. H. Guo, Y. L. Zhu, T. Yang and Z. D. Zhang, *Appl. Phys. Lett.* **97**, 172502 (2010).
81. M. Egilmez, R. Patterson, K. H. Chow and J. Jung, *Appl. Phys. Lett.* **90**, 232506 (2007).
82. X. W. Wu, M. S. Rzchowski, H. S. Wang and Q. Li, *Phys. Rev. B* **61**, 501 (2000).
83. R.-W. Li *et al.*, To be published.
84. I. Pallecchi, L. Pellegrino, E. Bellingeri, A. S. Siri, D. Marré, A. Tebano and G. Balestrino, *Phys. Rev. B* **78**, 024411 (2008).
85. X. Hong, J. B. Yau, J. D. Hoffman, C. H. Ahn, Y. Bason and L. Klein, *Phys. Rev. B* **74**, 174406 (2006).
86. A. P. Malozemoff, *Phys. Rev. B* **34**, 1853 (1986).
87. R. P. van Gorkom, J. Caro, T. M. Klapwijk and S. Radelaar, *Phys. Rev. B* **63**, 134432 (2001).
88. I. A. Campbell, A. Fert and O. Jaoul, *J. Phys. C: Solid State Phys.* **3**, S95 (1970).
89. M. Ziese, *Phys. Rev. B* **62**, 1044 (2000).
90. J. D. Fuhr, M. Granada, L. B. Steren and B. Alascio, *J. Phys.: Condes. Matter* **22**, 146001 (2010).
91. J. D. Fuhr, M. Avignon and B. Alascio, *Phys. Rev. Lett.* **100**, 216402 (2008).
92. G. Herranz, F. Sánchez, M. V. García-Cuenca, C. Ferrater, M. Varela, B. Martínez and J. Fontcuberta, *J. Magn. Magn. Mater.* **272–276**, **Part 1**, 517 (2004).
93. M. R. T. Venkatesan, Zi-Wen Dong, S. B. Ogale and R. Ramesh, *Proc. R. Soc. Lond. A* **356**, 1661 (1998).
94. E. Dagotto, *New J. Phys.* **7**, 67 (2005).